Int J Adv Manuf Technol (2012) 58:267–278
DOI 10.1007/s00170-011-3386-3

ORIGINAL ARTICLE

Drilling of woven glass fiber-reinforced plastic—an experimental and finite element study

Nilanjan Das Chakladar · Surjya K. Pal · Parthasarathi Mandal

Received: 28 July 2010 / Accepted: 9 May 2011 / Published online: 31 May 2011

Abstract Drilling in woven fiber-reinforced plastics is a well-known practice in modern-day manufacturing. The high fracture toughness of woven fiber-based composites over unidirectional counterparts is increasing demand in aviation and electronics industries. Hence, failure of these materials at harsh environments is a matter of concern. Very few numerical studies on drilling of these composites have been carried out; hence, the present scope may be considered as a trial de novo. Delamination was studied in the present work at different feed–speed combinations. Drilling responses were estimated using finite element as a numerical simulation tool. An equivalent elastic macromechanical model was assumed for the woven composite workpiece. A 3D drill bit was modeled using commercial CAD package Pro-Engineer and Ansys Autodyn was used as the solver environment. The simulation and validation experiments were carried out at planned feed–speed combinations. The effect of process parameters on exit and entry delamination is also documented. The thrust determined by finite element techniques showed good prediction with the experimental results.

Keywords Glass fiber-reinforced polymer (GFRP) · Drilling · Delamination

N. D. Chakladar · S. K. Pal (✉)
Department of Mechanical Engineering,
Indian Institute of Technology,
Kharagpur 721 302, India
e-mail: skpal@mech.iitkgp.ernet.in

P. Mandal
School of Mechanical, Aerospace and Civil Engineering,
The University of Manchester,
Manchester, UK

Nomenclature

h	Helix angle (degree)
l	Pitch of helix (millimeter)
$l_{\min}$	Minimum characteristic dimension of an element (millimeter)
p	Half-point angle (degree)
r	Instantaneous radius (millimeter)
Δt	Time step (second)
C	Tensor modulus (megapascals)
D	Drill diameter (millimeter)
$D_{\text{exit del}}$	Maximum exit delaminated diameter (millimeter)
D_{hole}	Hole diameter (millimeter)
E	Modulus of elasticity (gigapascals)
E_{11}	Elastic modulus along 11 (longitudinal) direction (gigapascals)
E_{22}	Elastic modulus along 22 (transverse) direction (gigapascals)
E_{33}	Elastic modulus along 33 (thickness) direction (gigapascals)
G_{12}	Shear modulus along 12 plane (gigapascals)
G_{23}	Shear modulus along 23 plane (gigapascals)
G_{13}	Shear modulus along 13 plane (gigapascals)
R	Drill radius (millimeter)
w	Web thickness (millimeter)
$\dot{\varepsilon}$	Strain rate (millimeter/millimeter/second)
ν_{12}	Poisson's ratio along 12 (−)
ν_{31}	Poisson's ratio along 31 (−)
ν_{23}	Poisson's ratio along 23 (−)
ρ	Density (kilogram per cubic meter)
$[\sigma]^n$	Calculated stress at nth cycle (megapascals)

1 Introduction

Machining composites is a prime concern in modern-day manufacturing due to non-homogeneity/anisotropy in material

properties. Making holes in fiber-reinforced plastic (FRP) are one of the important applications—hence, drilling of FRP is quite significant. From bolting assemblies in aviation industries to printed wiring boards in electronics, FRPs are used for high-specific strength and fracture toughness. Typically uncoated high-speed steel drill bits are used for conventional drilling of FRP, while cemented carbide drill bits are used for high-speed drilling. The FRPs are often used to reinforce steel structures by bolting arrangement. But to assemble these bolts, both steel and FRP structures are to be drilled, where during drilling due to material characteristics of FRP the drill bit rapidly wears which is a preliminary cause for FRP delamination. Drilling is itself a highly complicated dynamic process involving complex geometrical interactions, elasto-plastic failures, and friction. The same drill exhibits extrusion at the chisel edge and cutting action at the cutting lips leading to oblique cutting (due to change of rake and inclination angle) at the cutting lips and orthogonal cutting at the chisel edge. Hence, the basic requirement is to find out number of holes to be drilled with a fresh drill bit on FRPs and propose an optimum design and manufacturing of the drill bit. To design such a drill bit, prediction of wear and estimation of drilling response like thrust are indispensable.

FRP had its vital applications during post World War II in boat hulls, minesweeping vessels, bath tubs and covers, pressure vessels, submarine parts, aircraft components, etc. Since 1990, the thrust and cutting forces in drilling of unidirectional FRP composites are modeled and validated keeping in mind the basic idea of evaluating force through circular plate bending theories [1, 2]. The properties of woven composites make them more challenging for numerical modeling, compared to its unidirectional counterpart for same number of plies, material, and binding matrix. Meanwhile in 1996, the variation of thrust and torque with change in fiber angle for unidirectional composites was reported after taking video images through high-speed cameras at the onset of delamination [3]. In 2004, conventional drilling on composites was compared with oscillatory drilling and delayed tool wear was inferred with the oscillatory technique [4]. The extent of delamination in unidirectional carbon fiber based composite was analyzed using different types of drill—twist drill, saw drill, and candle stick drill where delamination due to candle stick drill was concluded to be minimum [5]. In recent years, effects of high speed in drilling of glass fiber-reinforced polymer (GFRP) were also studied and a model for adjusted delamination factor was introduced that considered a dimensionless factor compensating the total extent of delamination along the periphery [6].

A finite element analysis was carried out in 1992 to predict the load causing delamination in a quasi-isotropic graphite epoxy laminate with or without backing [7]. For angle ply laminates, a thrust force model was proposed along depth of the drilled hole in 1994 [8]. A quasi-3D orthotropic model was developed for estimation of element stiffness matrix and push-out delamination in the model was showed by the deletion of beam elements [9]. Later, six-node hexahedral element was considered to trace effective pattern of delamination than predicted by 20-node shell element [10]. However, the interlayer fracture toughness which was unknown till 2001 was finally analyzed by considering a double-beam cantilever structure for the composite plate to come up with interlayer separation [11]. Thus, the free-edge delamination of every laminate was investigated through evaluating the interlaminar tensile and compressive stresses [12].

The need for improved tool geometry for minimum delamination and hence minimum wear has led the present authors to begin this novel investigation of the machining responses while drilling woven composites using finite element techniques. But drilling being a very complicated machining process, it is difficult to address its geometry by an equivalent 2D plane strain model unlike orthogonal turning. Hence, near-precise modeling of drill bit is taken into consideration. We have tried to consider finite element modeling parameters realistic with the experimental setup and loading and boundary conditions for good prediction. The present scope is restricted to drilling thrust as the machining response as push-out/exit delamination is primarily responsible for catastrophic failure of these composites.

2 Experimental investigation

To observe the effect of process parameters on drilling thrust and torque and delamination, experimental studies were undertaken. A piezoelectric drill dynamometer (Kistler, 9272A), charge amplifier (Kistler, 5070A), and data acquisition card (NI, 6210) were used to capture and save signals using LabVIEW 7.1. The GFRP plate (100×50×9 mm) was not directly placed over the dynamometer but in between two mild steel (MS) plates with a central hole of 20-mm diameter. The MS plates were bolted together to ensure no relative movement as shown in Fig. 1.

Experiments were performed in Agni BMV 45 T20 CNC Machining Centre with simple computer numerical control codes suffice to carry out drilling at different speed–feed combinations. Finally, a MATLAB program [13] was written to find out the average drilling thrust force during the steady cutting period. This program took care of zero offset in the following way. The user selected two points in the fluctuating base voltage before the rise of signal and similar two points after the voltage drops, i.e., after hole machining, from which the average base voltage line was computed. Further, two extreme points were selected in the

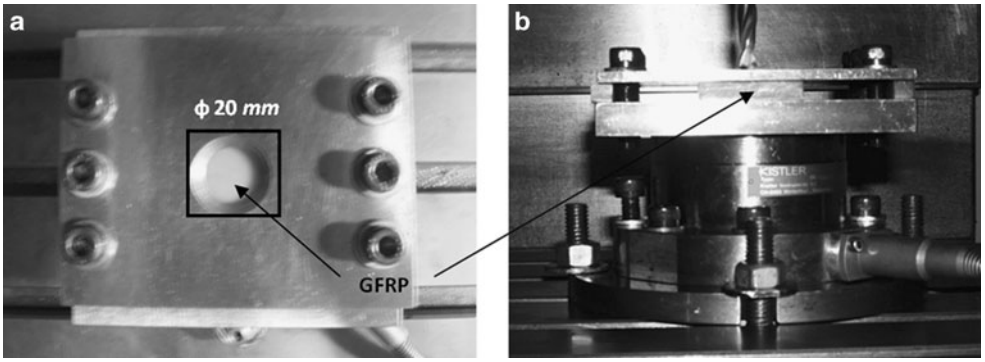

Fig. 1 **a** Work holding fixture and **b** dynamometer

steady zone and mean is evaluated of all signals lying between them. But this was not the true mean value for response; hence, it was compensated with zero offset depending whether the average baseline was above zero or below and finally this compensated average during steady cutting period multiplied with appropriate conversion factor (change in voltage to change in force (*N*)) gave corresponding drilling responses. The experimental studies were performed using two different types of drill bit—high-speed steel (HSS) and carbide as shown in Fig. 2. The specifications of HSS and carbide are listed in Table 1.

The workpiece used is GFRP with woven E-glass thermosetting epoxy laminate structure. The fiber strands in every layer of GFRP were distributed in two sets—one interweaving orthogonal to the other. The specifications of workpiece are listed (obtained from manufacturer's catalog, Sunrisefrp, Pune) in Table 2. The feed speed combinations are shown in Table 3.

The experimental setup has been depicted in the form of block diagram in Fig. 3 to identify the signal capturing and processing technique.

3 Geometric modeling of 3D drill bit

The accurate estimation of thrust force largely depends on precise modeling of drill bit and the work material. The geometry of chisel edge is the prime concern so far as thrust force is considered yet the fiber and matrix modeling need equal care.

Y-axis	Common perpendicular intersecting the extensions of cutting edges (see Fig. 4)
Z-axis	Parallel to the longitudinal axis of the drill
X-axis	Orthogonal to *Y*- and *Z*- axes

One quarter of the flute shape was formulated in the following polar equation [14] –

$$\psi = \sin^{-1}\frac{W}{2r} + \frac{\sqrt{r^2 - \left(\frac{W}{2}\right)^2}}{R}\tan h \cot p \tag{1}$$

Equation 1 was used as the parametric polar equation in Pro-Engineer [15], where *r* was varied from *W/2* to *R* (half of diameter of the drill). Thus, one quarter of the flute shape was produced in first quadrant of *XY* plane. The generated area was then mirrored about *X* and *Y* axis to develop the 2D surface in *XY* plane. The helix equation was parametrically written as follows:

$$\begin{aligned} r &= R \\ \theta &= -360tn \\ z &= -ltn, \end{aligned} \tag{2}$$

where *n*=number of turns in the helix, *l*=pitch of the helix, *t*= 0–1.

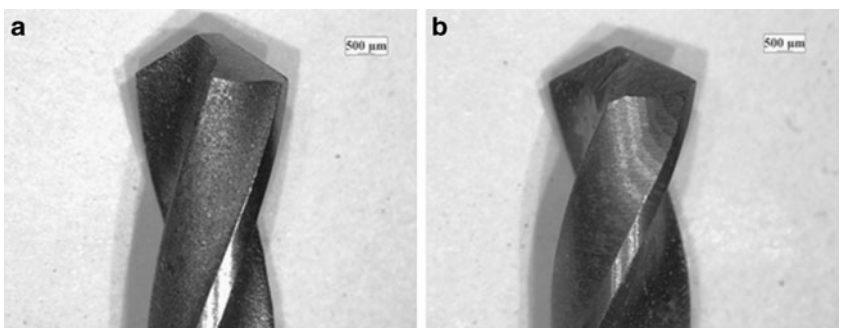

Fig. 2 **a** HSS and **b** carbide drill bits

Table 1 Specifications of HSS and carbide drill bit

Specifications	High-speed steel	Carbide
Density (kg/m^3)	7,860	11,560
Drill diameter (mm)	5	5
Helix angle (°)	30	30
Point angle (°)	118	130
Chisel edge radius (mm)	0.65	0.7
Chisel edge angle (°)	135	135
Lip relief angle (°)	12	12

Further, this flute profile was cut helically from the full-extruded part of the drill along the following curve

$$Z_{flute} = \frac{\tan h}{r} \times Z \tag{3}$$

$$h = \tan^{-1} \frac{2\pi r}{l} \tag{4}$$

where, Z_{flute} stands for longitudinal polar coordinate of helical flute.

Once the flute profile was finished, the flank shape was estimated through flank grinding assuming the grinding wheel was rotated about a fixed axis to form a "grinding cone" of cone angle α. To generate two flank surfaces, the grinding was performed twice from two symmetric positions to determine the right and left cones [16]. Flank surfaces are assumed to be the parts of the frustum of grinding cones. The three flank-grinding parameters were ϕ, d, and s, where ϕ was the rotation of coordinate system of the grinding cone such that the outer profile of the cone smoothly could meet the desired flank surface, d was the vertical distance from the chisel edge to the origin of newly rotated coordinate system, and finally the vertex was shifted to the right by a distance s in the Y-axis to generate right flank surface as listed in Table 4. The different steps for modeling of drill bit in Pro-Engineer are shown in Fig. 4.

Table 2 Specifications of GFRP workpiece

Specifications	GFRP
Specific gravity	1.68
Water absorption (% by weight)	0.07–0.08
Glass content (% by weight)	65–75
Fiber orientation	0°/90°

Table 3 Feed-speed combinations for experimental and simulation studies. For each type of drill bit there are eight feed–speed combinations

Feed (mm/rev)	Speed (m/min)	Type of drill bit
0.25		
0.50	45	High speed steel (ISO 235/1, AISI T4)
0.75	65	Carbide (ISO B978A03000, KC 7315)
1.00		

Similarly, it was the case with other flank surface with Z coordinate of the cone remaining same and interchanging the sign of X and Y coordinates. The schematic of drill modeling has been shown through the basics of drill grinding in Fig. 5.

After the virtual cone was generated, the profile was "revolved cut" from the earlier swept profile to obtain one flank surface. Since the margin was not considered in the present study, the final drill bit was modeled after two revolve cuts.

4 Geometric modeling of workpiece

In this research, delamination or chip formation was not taken into account; hence, an elastic macromechanical model for a woven composite was developed. The thickness of the workpiece model is kept at 2 mm such that at least one revolution of drill could be traced because maximum feed considered is 1.0 mm/rev. The outer dimensions of the geometric model are assumed to be a square domain of 20×20 mm keeping in mind the boundary conditions for experimental setup. Preliminary simulation studies with cylindrical domain revealed severe distortions on the boundaries for a circular model of workpiece due to the interference of stress waves leading to nonconvergence of the solution. These wave modes from FE analysis affected the stability of workpiece geometry. Hence for simplicity and avoiding such discrepancies, the workpiece in this work has been simplified with a rectangular block.

5 Finite element modeling

The finite element modeling is a well-established method for analyzing static or dynamic, linear or nonlinear responses on bodies subjected to varying loads. Solving problems that involve complex geometries, loading, boundary conditions, and complex contacts has made finite element an acceptable numerical simulation technique in

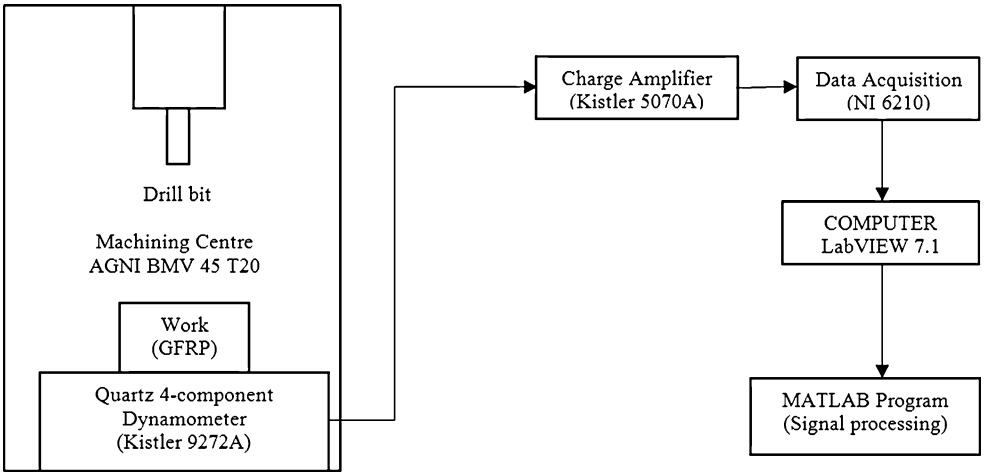

Fig. 3 Experimental block diagram

this field. Machining is such a complex analysis domain. To simplify the finite element analysis and save computation time, some important assumptions are considered, which may not fully simulate the realistic situation but suffice to judge the drilling phenomenon. The assumptions are stated below:

(a) The tool was considered as rigid.

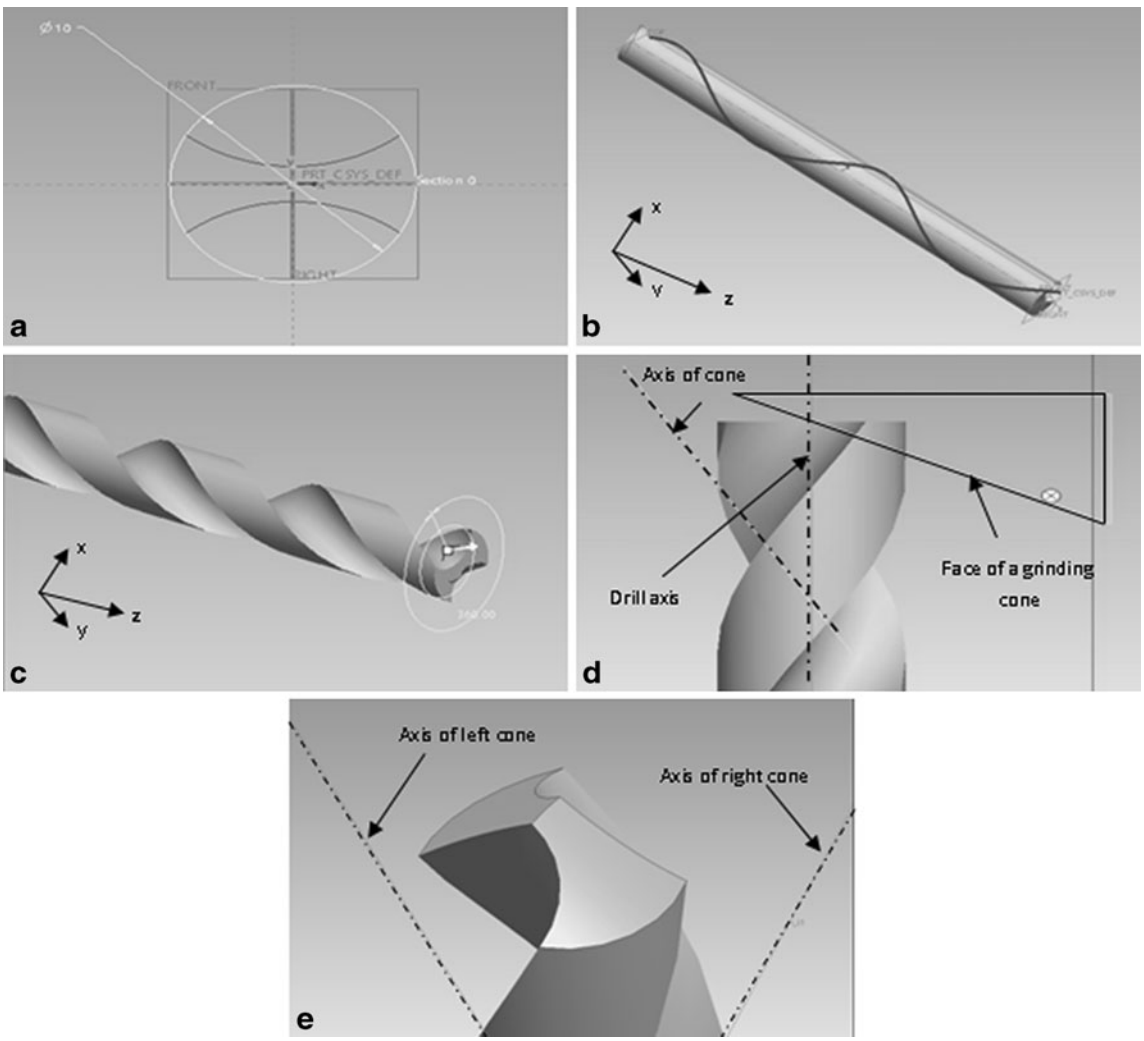

Fig. 4 Steps for modeling drill bit. **a** Flute cross-section, **b** helix profile of drill bit, **c** Boolean subtraction of helical flute, **d** axis of revolution and face of grinding cone, and **e** close-up view of chisel edge

Table 4 Manufacturing and geometric parameters for drill grinding

Manufacturing parameters	Values	Geometric parameters	Values
$R = D/2$	2.5 mm	d=1.9 D	9.5 mm
W=0.1D	0.5 mm	s=0.475 D	2.375 mm
D	5 mm	α	30°
p	59° (HSS)		
	65° (carbide)		

(b) In experimental setup, mild steel plates were kept at the top and bottom of the work plate with a centrally located hole of diameter 20 mm. Since it can be ensured that no large deformation would take place at the periphery of this hole while drilling a hole of 5 mm, hence, for finite element study, a 20-mm square plate was considered with all the four outer boundary planes constrained in all directions including rotations.

(c) The actual model of drill bit had a length of 75 mm; but from computational time perspective and as the chips are mostly in the form of powders, the long helical flute can be eliminated and an appropriate height of 15 mm above the cutting edge was considered.

(d) The average thrust was taken as the sum of the reactions obtained at the boundary nodes in Z direction over steady zone.

(e) Since elastic behavior was assumed for workpiece and actual chip model is not taken into account, damage/failure model is not used and interaction is considered frictionless.

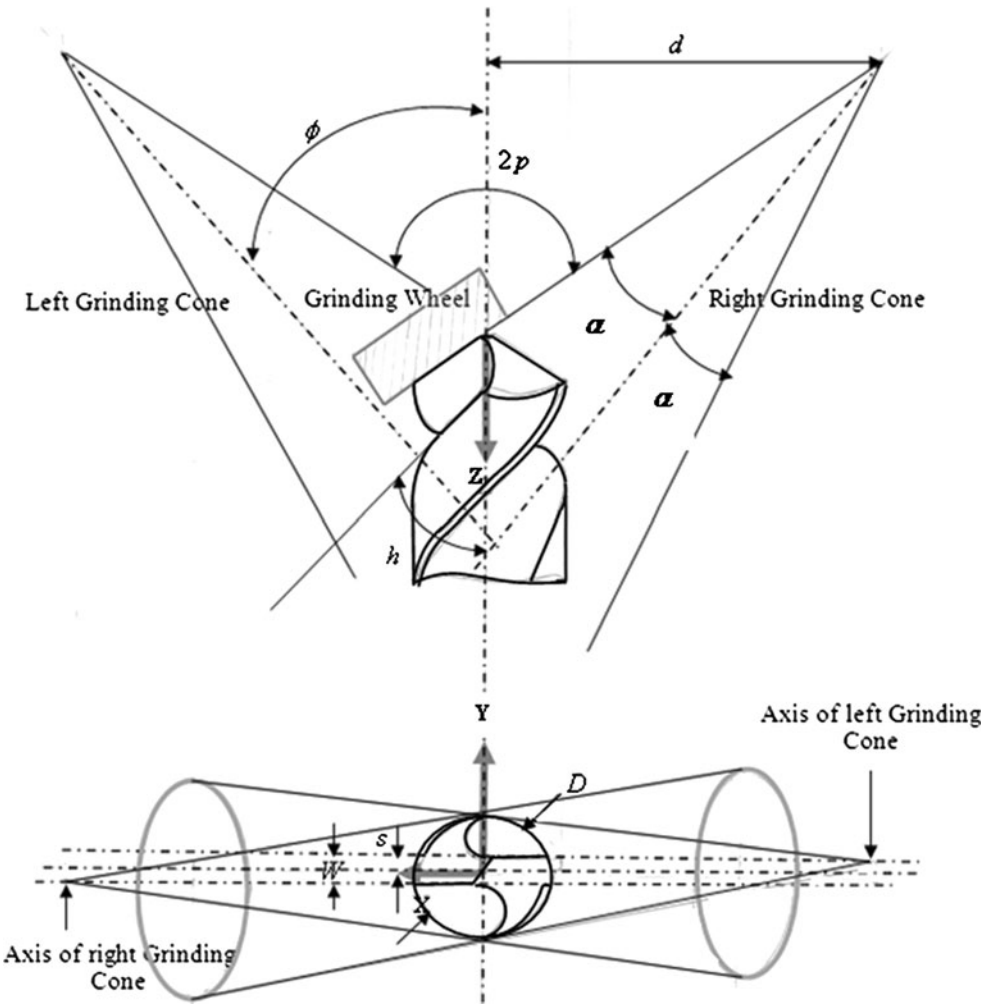

Fig. 5 Schematic of drill grinding

5.1 Meshing of drill bit and work

The tool geometry was exported from computer-aided design package in Initial Graphics Exchange Specification format to Ansys Workbench v12.0.1 for meshing. The tool was meshed with four-node linear tetrahedral rigid elements of average element size 0.4 mm. A mesh refinement was done only at the chisel edge to accurately identify the displacement field at the edge of contact with a refinement ratio (coarse/fine, 1.0:0.5). Total number of elements used to mesh the tool is 8,376. The work was meshed with 27,530 ten-noded (four corner nodes and six mid-side nodes) tetrahedral elements of average dimension 0.2 mm.

5.2 Material constitutive model

The material model used for workpiece was orthotropic elastic. The data used for orthotropic model follows in Table 5 [17]:

A macromechanical approach was used to predict thrust during drilling the composite material. The anisotropic material was represented by an equivalent homogenous model for the present study. This can be justified as chip formation is not modeled.

As epoxy resin matrix is of thermosetting type, it shows mostly glassy phase in the machining domain hence the material deformation can well be considered within elastic regime. So the material model has been chosen orthotropic and elastic for the workpiece.

Summerscales rule of equivalence was used to find equivalent bulk modulus for an orthotropic material [18] required to compute incremental time step for the finite element analysis.

$$K_{eq} = \frac{\sqrt[3]{E_{11}.E_{22}.E_{33}}}{3(1-2.\sqrt[3]{\nu_{12}.\nu_{31}.\nu_{23}})} = 10.387\,GPa \tag{5}$$

Equation 5 reduces to traditional isotropic form when $E_{11}=E_{22}=E_{33}$ and $\nu_{12}=\nu_{31}=\nu_{23}$.

Constitutive equation for incremental stress update scheme shown in Eq. 6 [19]:

$$[\sigma]^{n+1} = [\sigma]^{n} + [C][\dot{\varepsilon}]\Delta t \tag{6}$$

Table 5 Constitutive properties for woven GFRP composite

Elastic modulus (GPa)		Poisson's ratios		Shear modulus (GPa)	
Notations	Values	Notations	Values	Notations	Values
E_{11}	21	ν_{12}	0.26	G_{12}	1.52
E_{22}	21	ν_{23}	0.26	G_{23}	1.52
E_{33}	7	ν_{13}	0.30	G_{13}	2.65

$$S = C^{-1} = \begin{bmatrix} \frac{1}{E_{11}} & \frac{-\nu_{12}}{E_{11}} & \frac{-\nu_{31}}{E_{33}} & 0 & 0 & 0 \\ \frac{-\nu_{12}}{E_{11}} & \frac{1}{E_{22}} & \frac{-\nu_{23}}{E_{22}} & 0 & 0 & 0 \\ \frac{-\nu_{31}}{E_{33}} & \frac{-\nu_{23}}{E_{22}} & \frac{1}{E_{33}} & 0 & 0 & 0 \\ 0 & 0 & 0 & \frac{1}{2G_{12}} & 0 & 0 \\ 0 & 0 & 0 & 0 & \frac{1}{2G_{23}} & 0 \\ 0 & 0 & 0 & 0 & 0 & \frac{1}{2G_{31}} \end{bmatrix} \tag{7}$$

5.3 Solver methodology

The present research work incorporated a new explicit remeshing scheme to control hourglassing while using reduced integration mid-side-noded elements which is commercially available in FE package Ansys Autodyn 12.0.1. Traditionally, the literature has documented use of Arbitrary Lagrangian Eulerian solver for machining or large strain rate (large deformation) problems to control high mesh distortion. But it is seen that such solvers take high computational time and effort. Moreover, such algorithms involve lot of other parameters like remesh sweep, number of iterations per increment, advection parameters, and so on. As a result, proper choice of these factors is equally important. The solver technique utilized in present study was average nodal pressure (ANP) technique. The methodology incorporated in this strategy was as follows.

For a standard four-noded tetrahedron, initial geometry of element (e) was interpolated using isoparametric coordinates (ξ_1, ξ_2, ξ_3) as

$$X^{(e)} = \sum_{a=1}^{4} N_a(\xi_1,\xi_2,\xi_3)X_a \tag{8}$$

where N_a denotes the shape function for local node a which varies from 1 to 4 [20]. Later, a 10-noded quadratic tetrahedron was considered to incorporate the remeshing technique as shown in Fig. 6a.

The solver also took care of lumped mass matrix typically employed in explicit dynamic applications. Here, the governing equations at any instant of time was represented by nodal equilibrium equation for a given mesh node a is

$$M_a a_a = F_a - T_a \tag{9}$$

$$M_a = \sum_{e=1}^{m_a} M_a{}^{(e)} \tag{10}$$

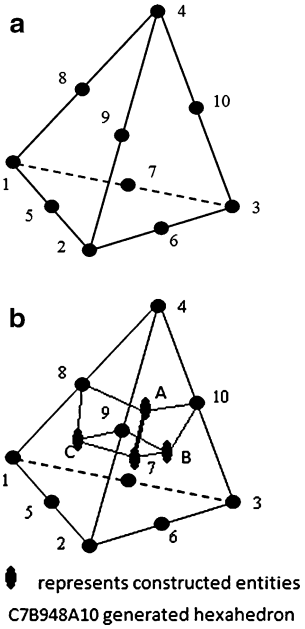

Fig. 6 **a** Ten-noded quadratic tetrahedron, **b** hexahedron generated from tetrahedron

$$M_a^{(e)} = \int_{V^{(e)}} \rho_o N_a dV = \frac{1}{4}\rho_o{}^{(e)} V^{(e)} \tag{11}$$

where, $M_a$represents assembled lumped mass at node a, $F_a$equivalent nodal external force, $T_a$is the equivalent nodal internal force due to body stress, $a_a$is the acceleration vector of node a, ρ_o is density, and $V^{(e)}$ is the elemental volume.

Each elemental contribution was attributed by integrating shape function corresponding for node a over mass of the element to give lumped nodal mass and finally average nodal volume was evaluated. The remeshing technique utilized in this scheme divides a 10-noded tetrahedron into four hexahedrons by constituting eight corner nodes of hexahedron from three circumcenters of triangular faces attached to the corner node under consideration, one centroid of tetrahedron, three mid-side nodes of edges adjacent to the corner node and the corner node itself as shown in Fig. 6b. A brief explanation has been documented for average nodal pressure formulation how the volumetric strain energy is approximated to avoid large number of constraints that are encountered in standard formulation. The volumetric strain energy $\Pi_{\text{vol}}(x)$ is evaluated as

$$\Pi_{\text{vol}}(x) = \sum_{a=1}^{4} U(J_a) V_a \tag{12}$$

$$J_a = \frac{v_a}{V_a} \tag{13}$$

where, J_a is the volumetric ratio, $U(J_a)$represents the volumetric component of strain energy density function depending on volumetric ratio, $v_a$current element volume and $V_a$is the initial element volume. Once this volumetric strain energy was determined, corresponding volumetric internal virtual work δW_{vol} was evaluated from

$$\delta W_{\text{vol}} = D\Pi_{\text{vol}}[\delta v] = \sum_{a=1}^{n} p_a V_a D J_a[\delta v] \tag{14}$$

$$p_a = \left.\frac{dU}{dJ}\right|_{J_a=\frac{v_a}{V_a}} = k\left(\frac{v_a - V_a}{V_a}\right), \tag{15}$$

where, p_a is the average nodal pressure, $D\Pi_{\text{vol}}[\delta v]$ denotes differentiation of volumetric strain energy, and k is bulk modulus.

The directional derivative of the average nodal volumetric strain was obtained using definition of nodal volumes which finally enables the equation for volumetric component of internal virtual work, δW_{vol} as

$$\begin{aligned}\delta W_{\text{vol}} &= \sum_{a=1}^{4}\sum_{e=1}^{m_a} \frac{1}{4} p_a v^{(e)} \operatorname{div} \delta v^{(e)} \\ &= \sum_{e=1}^{m_a} \overline{p}^{(e)} v^{(e)} \operatorname{div} \delta v^{(e)}\end{aligned} \tag{16}$$

Thus, the average element pressure, $\overline{p}^{(e)}$, can be assumed to be the pressure acting at the centroid of the element which can be equated to the pressure obtained from linear interpolation of nodal values.

$$\overline{p}^{(e)} = \frac{1}{4}\sum_{a=1}^{m_a} p_a{}^{(e)} \tag{17}$$

6 Experimental results and discussion on delamination

The delamination damages normally observed in drilling of laminated composites are of two types—exit or push-out and entry or peel-up. The exit delamination is found to be more detrimental than peel-up as it leads to catastrophic failure of the composite material. The chips are mostly in powdery form since the fiber and matrix are prone to brittle fracture. But at high speed and low feed, the chips are in the continuous regime where due to high temperature, matrix melts and gets softened thus reducing the thrust force and the broken chips get hardened due to high-temperature gradient.

The delamination is evaluated by a dimensionless factor represented by $\text{DF} = \frac{\pi D_{\text{exit del}}{}^2/4}{\pi D_{\text{hole}}{}^2/4}$, and was measured using stereo zoom microscope (Leica, DFC 295), as shown in Fig. 7. Peel-up and push-out delamination factors have been plotted against the process parameters as shown in Fig. 8.

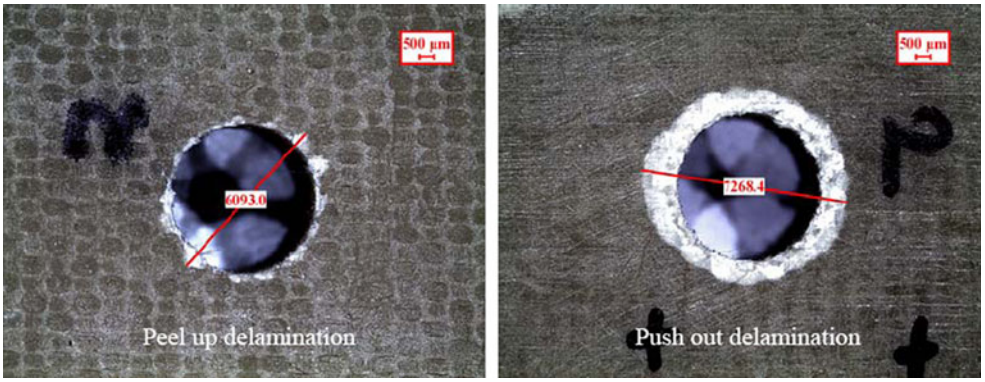

Fig. 7 Measurement of delamination at V_c=45 m/min and s= 0.5 mm/rev using carbide drill bit

Carbide tools are more preferable for high speed machining than HSS for their hot hardness and material rigidity which reduces the responses, and hence delamination reduces in case of carbide than HSS. In Fig. 8a, at high cutting velocity and higher feed, the powdery chips are found to get hardened and thus clog with the penetration of

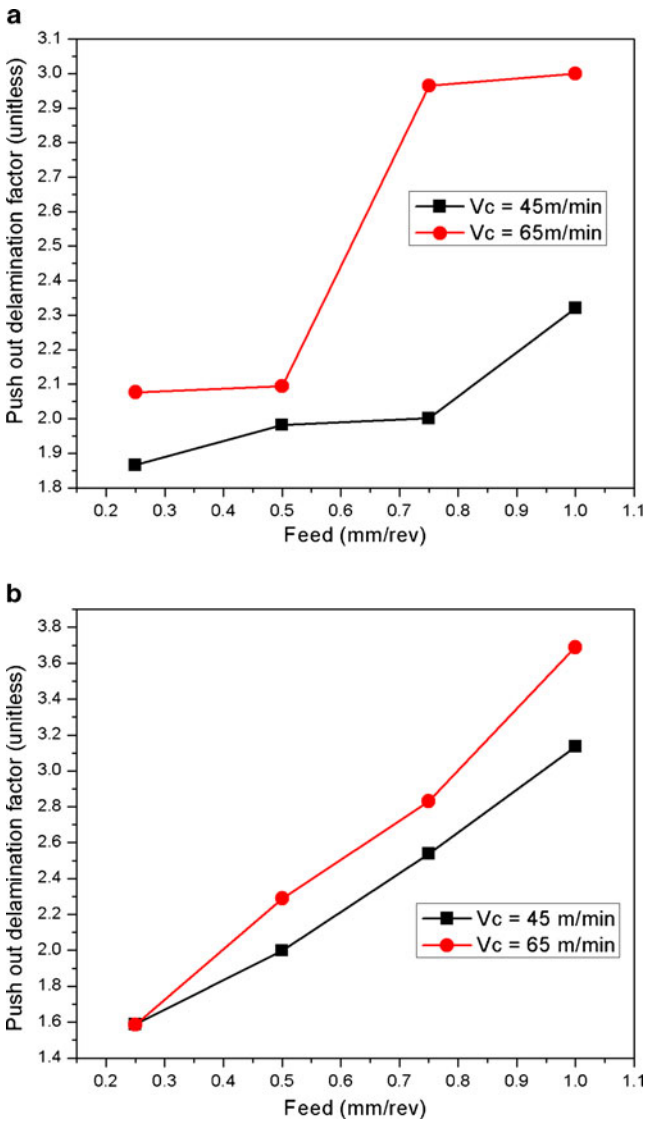

Fig. 8 **a** Exit delamination versus feed for HSS at V_c=45 and 65 m/min. **b** Exit delamination versus feed for carbide at V_c=45 and 65 m/min

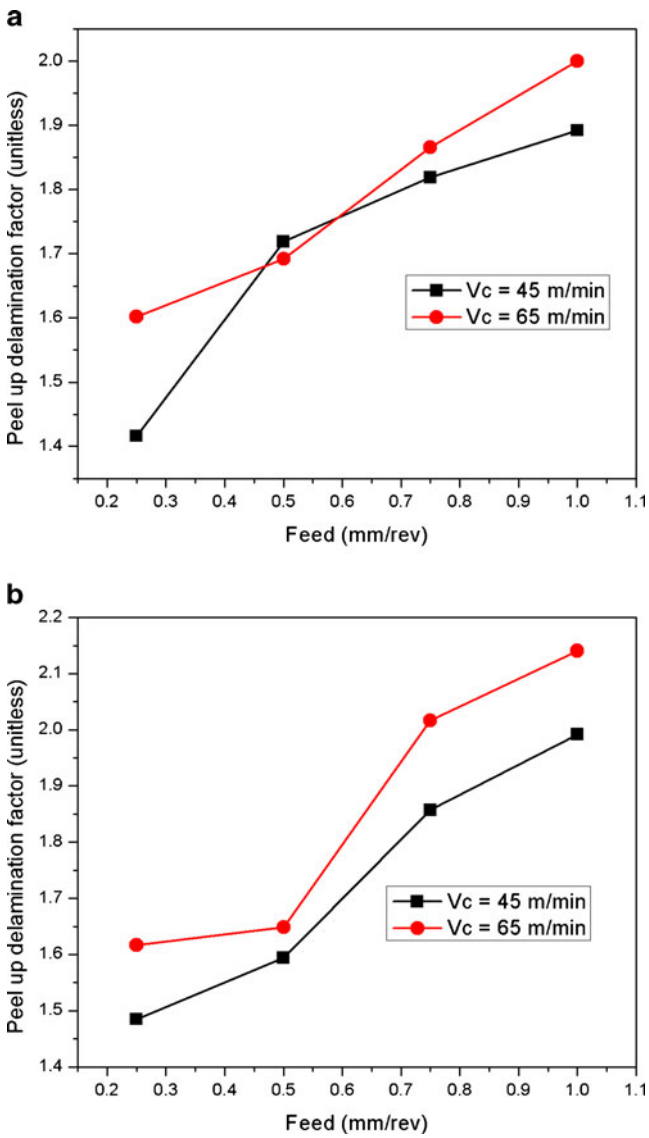

Fig. 9 **a** Peel-up delamination versus feed for HSS at V_c=45 and 65 m/min. **b** Peel-up delamination versus feed for carbide at V_c=45 and 65 m/min

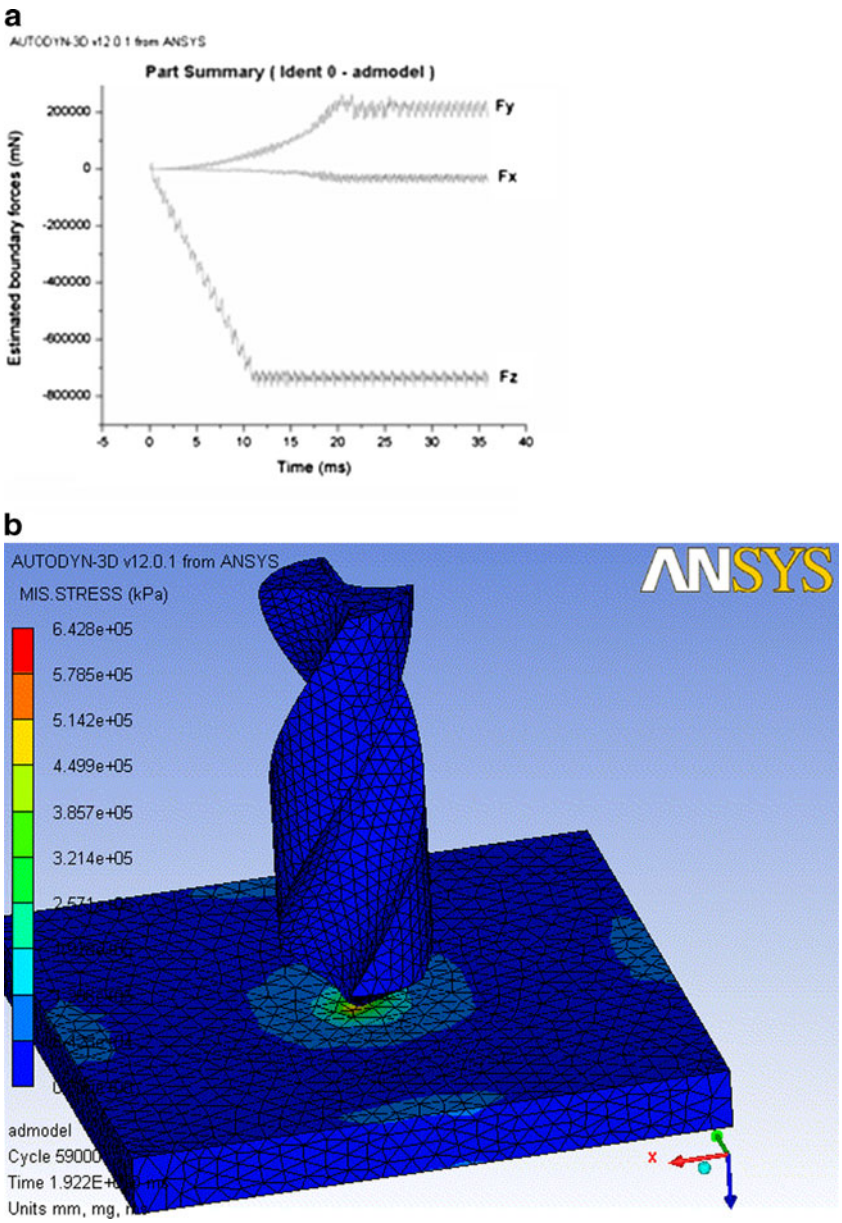

Fig. 10 **a** Estimated force signals at feed 0.75 mm/rev and V_c=45 m/min at t= 19.22 ms using HSS drill bit. **b** Contour plot of von Mises' stress at feed 0.75 mm/rev and V_c=45 m/min at t= 19.22 ms using HSS drill bit

drill increasing thrust and hence exit delamination. But contrary to tradition, the higher values of delamination at high feeds in Fig. 8b, signify the effect of drill point geometry into picture other than material properties of carbide. Because the higher the point angle, the higher is the push-out delamination. While in Fig. 9a, b, peel-up delaminations showed gradual increasing trend as it is mostly influenced by rotational speed.

7 Experimental versus finite element results and discussion

The material model in the finite element analysis is assumed as elastic; hence, only thrust force can be captured numerically. From previous studies, it is well documented that the thrust force can be captured by elastic bending of material under the type of loading it is subjected to. The estimated thrust is considered to be the sum of reactions of all boundary nodes along Z direction (opposite to direction of feed) during steady cutting period. The estimated force signals and a contour plot of von Mises' stress has been shown at feed 0.75 mm/rev and V_c=45 m/min at t= 19.22 ms for HSS drill in Fig. 10a, b. As material damage model is not incorporated in the finite-element analysis, the maximum von Mises' stress is found to be 642.8 MPa which is higher than the failure strength of work material. The assumption for considering drill as rigid, justifies the blue color for the entire drill bit stating zero stress. Maximum von Mises'

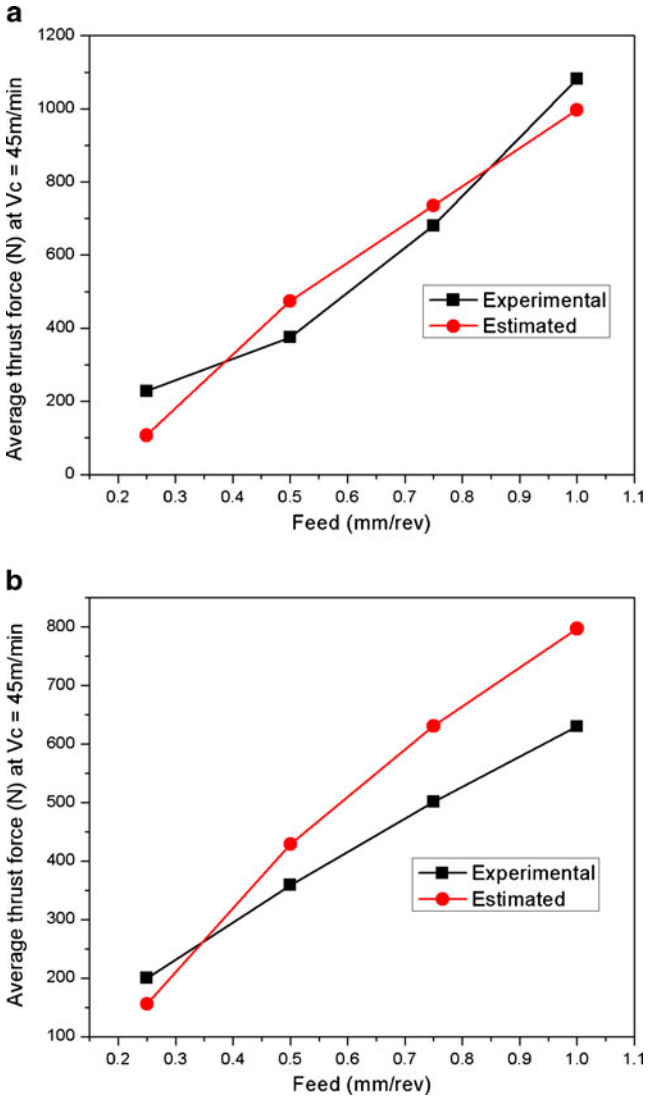

Fig. 11 **a** Comparison plots of thrust force for HSS drill bit at V_c=45 m/min. **b** Comparison plots of thrust force for carbide drill bit at V_c=45 m/min

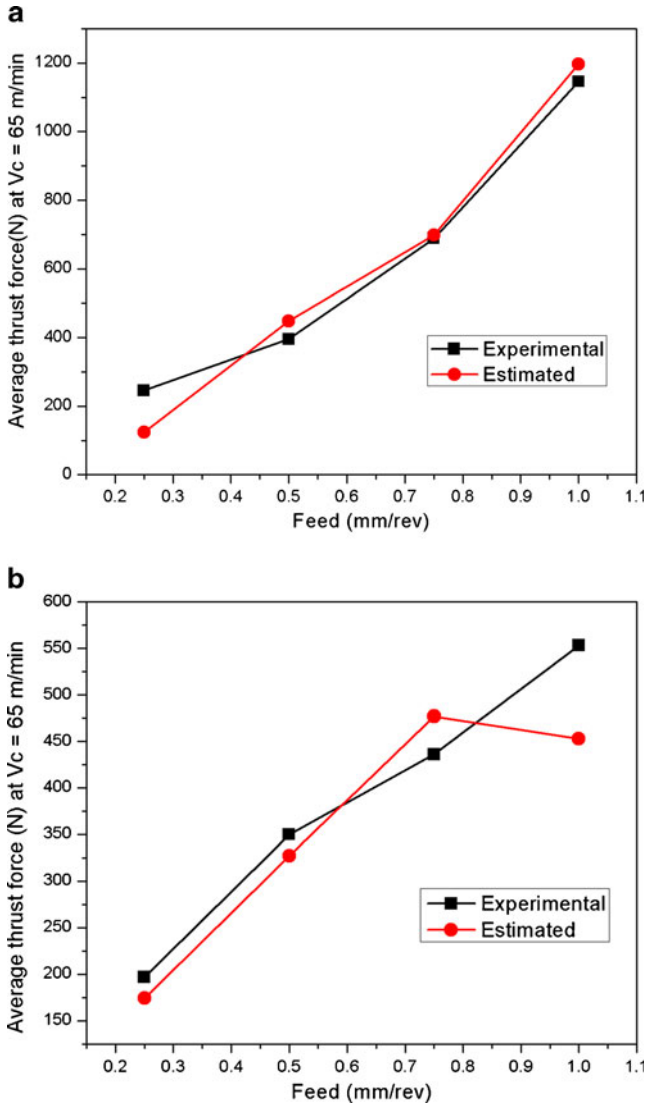

Fig. 12 **a** Comparison plots of thrust force for HSS drill bit at V_c=65 m/min. **b** Comparison plots of thrust force for carbide drill bit at V_c=65 m/min

stress occurs at the point of interaction of chisel edge and work material.

The comparison plots for experimental and finite element results show a near-estimate of drilling thrust with deviations ranging from 10% to 21% for lower cutting speeds of 45 m/min (Fig. 11a for HSS, Fig. 11b for carbide) using both the drill bits whilst 6–27% for higher cutting speed of 65 m/min as in Fig. 12a for HSS, and Fig. 12b for carbide. This deviations are due to important reasons like material constitutive properties are taken from literature, precise modeling of chisel edge and elastic material model for composites. In Fig. 13, two comparisons have been shown for change of simulated average thrust force with change in cutting speed and change in point angle of carbide drill bit. The graph shows at maximum cutting speed and minimum point angle the fiber rupture by the

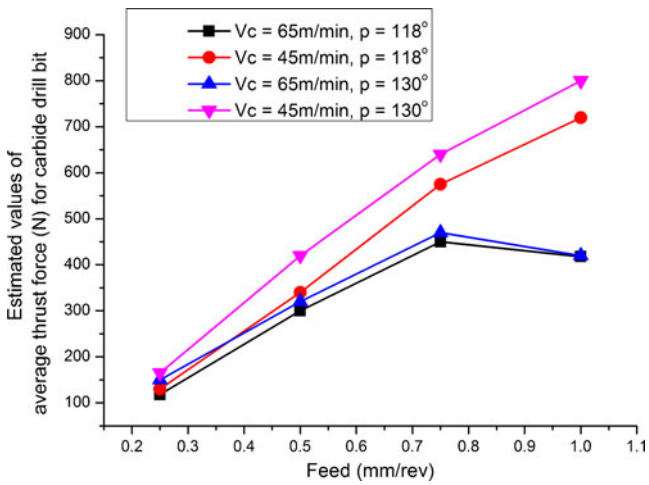

Fig. 13 Comparison plots of simulated thrust force for carbide drill bit with varying cutting speed and point angles

carbide drill bit is quicker with much reduced thrust force which accounts to the material properties of the drill bit and geometrical specification of drill angles. The thrust values at V_c=65 m/min for 118° point angle in Fig. 13 are less than that for 130° point angle which in turn are lower than the values seen in Fig. 12a, b. Although, at higher values of feed, problems like mesh distortions and hourglassing did affect the gradual trend in the simulated results. These inferences revalidate that carbide drills are more preferable in comparison to HSS drill bits during drilling of GFRP.

8 Conclusion and future scope

Among 16 holes drilled in the workpiece with HSS drill bit, the holes for V_c=45 and 65 m/min with same feed of 0.25 mm/rev showed minimum delamination (peel-up and push-out). But the rest from feed 0.5–1.0 mm/rev showed significant changes indicating that the tool has already started to wear; i.e., if a fresh drill bit is able to make a single hole, then the number of drills required is equal to the number of holes to be drilled or number of times the tool has to be reground. The rest 16 holes drilled with carbide drill bit showed comparatively less delamination than with HSS due to reduced thrust at same feed–speed combinations. High fracture toughness of work material has become the key reason behind drill wear, specifically at chisel edge which ultimately aggravates delamination and hence strength of the work material. So the present scope is a forerunner in achieving the same goal but for woven composites.

Though as a whole, the finite element analysis of drilling woven composites is highly complicated, the element shape function and the boundary conditions are simplified to save computation time. The motion constraints to workpiece and tool are kept as in experimental setup. A near-accurate 3D drill model has been developed based on available drill grinding techniques. The material model has been considered elastic which accounts to a close estimate of thrust within about 80–90% of the experimental values. An equivalent macromechanical model has been represented for the composite material which is sufficient to investigate the drilling responses. The ANP technique as finite element solver is found to work well with the present nonlinear analysis. As the material model is assumed as elastic, cutting action could not be predicted. Elastoplastic material model is essential to simulate actual cutting and chip formation finally leading to modeling of delamination. Softwares like Ultimatte AdvantEdge do simulate such elastoplastic deformation mechanisms but presently for metals. Hence, modeling such deformation problems can be accounted in future with proper subroutines to take care anisotropic failure phenomenon. Since the drill is considered rigid in the present study, the elements meshing the drill help only to compute mass inertia for finite element analysis. The drill profile acts only as a displacement field hence constitutive properties are not required. Modeling drill wear with deformable tool will include constitutive properties that can be kept as future scope.

References

1. Reedy ED, Mello FJ (1986) Modeling delamination growth in composites. Sandia National Laboratories, Albuquerque, NM, USA
2. Ho-cheng H, Dharan CKH (1990) Delamination during drilling in composite laminates. J Eng Ind 112:236–239
3. DiPaolo G, Kapoor SG, Devor RE (1996) An experimental investigation of the crack growth phenomenon for drilling of fibre-reinforced composite materials. ASME J Engg Ind 118:104–110
4. Ramkumar J, Aravindan S, Malhotra SK, Krishnamurthy R (2004) An enhancement of the machining performance of GFRP by oscillatory drilling. Int J Adv Manuf Tech 23:240–244
5. Hocheng H, Tsao CC (2003) Comprehensive analysis of delamination in drilling of composite materials with various drill bits. J Mat Proc Tech 140:335–339
6. Rubio JC, Abrao AM, Faria PE, Correia AE, Davim JP (2008) Effects of high speed in the drilling of glass fibre reinforced plastic: evaluation of the delamination factor. Int J Mach Tool Manuf 48:715–720
7. Sadat AB, Chan WS, Wang BP (1992) Delamination of graphite/epoxy laminate during drilling operation. J Energy Resour Technol 114:139–141
8. Jain S, Yang DCH (1994) Delamination of free drilling of composite laminates. J Eng Ind 116:475–481
9. Nishiwaki T, Yokoyama A, Maekawa ZI, Hamada H (1995) A new numerical modeling for laminated composites. J Compos Struct 32:641–647
10. Gruttmann F, Wagner W (2001) A finite element model for the analysis of delaminations in FRP-Shells, Trends in Computational Structural Mechanics, International Center for Numerical Methods in Engineering (CIMNE) Barcelona, 307–316.
11. Tanzawa Y, Watanabe N, Ishikawa T (2001) FEM simulation of modified DCB test for 3D orthogonal interlocked fabric composites. Compos Sci Technol 61:1097–1107
12. Goerguelue U (2009) Investigation of free edge delamination. Available from: http://www.gorgulu-home.com/Index_files/Pages/Useful_Notes/studies/Useful_notes/composites/Investigation_of_free_edge_delamination.pdf. Accessed 04 Aug 2009.
13. Matlab 7.1.0.246(R14), Mathworks Inc.
14. Vijayaraghavan A, Dornfeld DA (2007) Automated drill modeling for drilling process simulation. J Comput Inf Sci Engg 7(3):276–282
15. Pro-Engineer v2.0.
16. Kyratsis P, Bilalis N, Antoniadis A (2009) CAD based predictive models of the undeformed chip geometry in drilling. World Acad Sci Eng Technol 52:318–324
17. Sundarraja MC, Rajamohan S (2008) Flexural strengthening effect on RC beams by bonded composite fabrics. J Reinf Plast Compos 27:1497–1513. doi:10.1177/0731684407081377
18. http://www.tech.plym.ac.uk/sme/MATS324/MATS324A2%20E-G-nu.htm#K. Accessed on 08 Oct 2009.
19. Ansys Workbench 12.0.1 and Ansys Autodyn 12.0.1.
20. Bonet J, Burton AJ (1998) A simple average nodal pressure tetrahedral element for incompressible and nearly incompressible dynamic explicit applications. Comm Num Meth Engg 14:437–449